

Case History

Geometry of ophiolites in eastern Cuba from 3D inversion of aeromagnetic data, constrained by surface geology

José A. Batista-Rodríguez¹, Marco A. Pérez-Flores²,
Gerardo Quiroga-Goode³, and Luis A. Gallardo²

ABSTRACT

This study combined geophysical, geologic, and topographic information to investigate the Mayarí-Baracoa ophiolitic belt in eastern Cuba. A recently developed interpretation technique for 3D inversion of magnetic data was employed to determine the geometry at depth of ophiolitic and other rocks. Based on measured susceptibilities, lithologies were divided into four groups. The geophysical data allowed 3D imaging of ophiolites (serpentinized peridotites and gabbros), as well as sedimentary and volcanic rocks. The study verified that both the Pinares de Mayarí Plateau and the Sagua de Tánamo Basin have been strongly influenced by tectonic activity. The modeling showed evidence of more east-west structural deformation of the ophiolite belt than had been previously reported. The depth of the depocenter of the Sagua de Tánamo basin and its rate of subsidence were determined. We identified some areas with potential for economic deposits of chromium, cobalt, and nickel, as well as precious metals; these were related to the thickness of the peridotite layer. The modeling also corroborated the presence of previously mapped faults and revealed other previously unrecognized faults.

INTRODUCTION

The study area occupies an area of approximately 2754 km² adjacent to the northern coast of southeastern Cuba (Figure 1). Previous geologic and geophysical studies have focused principally on local exploration for lateritic Fe-Ni-Co and chromite deposits (Chang

et al., 1990; Chang et al., 1991). Some qualitative geologic interpretation has been carried out and 2D models have been developed from aeromagnetic profiles (Batista et al. 2002). Figure 2 shows a model proposed by Batista (2002); that correlates surface geology and the observed magnetic anomalies. Figure 1 shows the surface geology, including the distribution of serpentinized rocks and weathered crust, gabbros, volcanic rocks, and the locations of faults and dikes. From the work of Batista (2002), it appears that hydrothermal alteration is associated with faults. However, the results of these previous studies provide only a qualitative view. Therefore, the purpose of this study was to determine the geometry at depth of ophiolitic and other rocks by applying a 3D inversion method that allows quantitative interpretation of the magnetic field data.

The 3D inversion method we used was developed by Gallardo et al. (2003, 2005). It minimizes the quadratic norm of the differences between the data and model responses, and includes a measure of the model roughness, subject to constraints at every cubic cell. These constraints were used to introduce surface geologic data into the inversion process. Each rock group is represented by a set of rectangular prisms. The inversion process allows the removal of upper-layer prisms to represent intrusion from below, and to show outcrop where surface geology indicates that this is the case. Non-uniqueness is a problem in every geophysical method, but in potential field methods it is particularly serious because there is only a single measurement at every recording site, whereas in EM or seismic methods there is information for different frequencies or times. Our approach was to introduce surface geologic information in order to reduce, to some degree, this nonuniqueness, and to guide the solution toward a model that was consistent with the available geologic data.

Aeromagnetic data was collected by a Russian crew in 1990 at a height of 70 m, with a sampling rate of 10 m along the profiles (Chang et al., 1990). Because the data included a very high frequen-

Manuscript received by the Editor December 14, 2005; revised manuscript received December 11, 2006; published online April 27, 2007.

¹Instituto Superior Minero Metalúrgico de Moa, Las Coloradas, Mao, Holguín, Cuba. E-mail: jabatista@yahoo.com.

²CICESE, Departamento Geofísica Aplicada, Ensenada, México. E-mail: mperez@cicese.mx.

³Universidad Autónoma de Tamaulipas, Instituto de Investigación en Ingeniería, Tampico, México. E-mail: gquirogagoode@netscape.net.

© 2007 Society of Exploration Geophysicists. All rights reserved.

cy component, the contractor smoothed the data by upward continuation. Consequently, only an 850-m upward-continued grid was available in digital form.

Despite the loss of information because of upward continuation, prisms with horizontal dimensions of 2×2 km were used in the modeling to provide acceptable resolution at depth. Because of the long east-west dimension of the study area, the linear system of equations was unmanageable for 2×2 km prisms. Therefore, to avoid loss of resolution in the modeling we divided the study area into three sectors (Figure 1) according to their geologic characteristics. The Mayari and Sagua sectors are areas of topographically similar high massifs, and the Moa sector is dominated by a well-defined basin.

GEOLOGIC SETTING

Ophiolites are the dominant rocks outcropping in the study area, with minor amounts of sedimentary and volcanics from the Cretaceous and Paleocene (Figure 1) (Iturralde-Vinent, 1996). The ophiolites belong to the Mayari-Baracoa Ophiolitic Belt (Iturralde-Vinent, 1994, 1996). The main outcrops are the Mayari-Cristal and

Moa-Baracoa massifs (Proenza et al., 1999). The ophiolitic belt constitutes an allochthonous tabular body with a length of approximately 170 km, overthrusting the volcano-sedimentary and sedimentary rocks of the Upper Cretaceous. The ophiolites are overlain by volcano-sedimentary rocks of a Paleogene back-arc margin and by younger sequences of carbonate-terrigenous rocks (Cobiella, 2000).

Serpentinized peridotites overlain by gabbros constitute the typical ophiolitic sequence of the region. The accretion of the ophiolites from south to north was interpreted from regional seismic profiles acquired over northern Cuba (Iturralde-Vinent, 1996; Echevarria-Rodríguez et al., 1991), which showed a fold belt thrusting onto the northern platform edge of the island.

The study area is characterized by northeast- and northwest-trending faults, with both steep and shallow fault planes, that form a mesh of blocks and micro-blocks with differential movements between them (Figure 1). Most of the faults are normal (Campos, 1983; Rodríguez, 1998). Very complex folding is observed at the tectonic contacts (Campos, 1983). The contact between gabbros and serpentinized peridotites is normally tectonic. The peridotites and volcano-sedimentary rocks share a tectonic contact in some places (Iturralde-Vinent, 1996).

INVERSE METHOD

We used the total magnetic field from a rectangular prism (Bhattacharyya, 1966). We assumed that rocks with similar magnetic susceptibility form a single group, which we represented by an array of contiguous prisms. Where magnetic contrasts existed between the rocks, new groups were defined. Every group had a 3D top and bottom topography. The bottom of each group was coincident with the top of the underlying group. Initially, each group was assigned a constant thickness. As iterations advanced, each group deformed tri-dimensionally with no empty spaces between them. Iterations were stopped when the model response fitted the data within a specified misfit. The inversion was linear with respect to the magnetization vector, but nonlinear with respect to the depths of the prisms; therefore, a Taylor expansion was needed to linearize the inversion.

$$\mathbf{T}(\mathbf{m}) \cong \mathbf{T}(\mathbf{m}_0) + \mathbf{A}(\mathbf{m}_0)[\mathbf{m} - \mathbf{m}_0], \quad (1)$$

where $\mathbf{T}(\mathbf{m})$ is the scalar magnitude of the measured magnetic anomaly vector, $\mathbf{T}(\mathbf{m}_0)$ is the magnetic anomaly due to the initial or previous model, $\mathbf{A}(\mathbf{m}_0)$ is a rectangular matrix that contains the partial derivatives of the magnetic anomaly with respect to the top and bottom depth of every prism, \mathbf{m}_0 is a vector with the depths of every prism for an initial model, and \mathbf{m} is the vector of unknown depths. These unknowns were determined at every iteration and they converged when $\mathbf{T}(\mathbf{m}_0)$ fitted the measured $\mathbf{T}(\mathbf{m})$. The analytical form of $\mathbf{T}(\mathbf{m})$ can be found in Gallardo et al. (2005) and the derivatives in Gallardo et al. (2003).

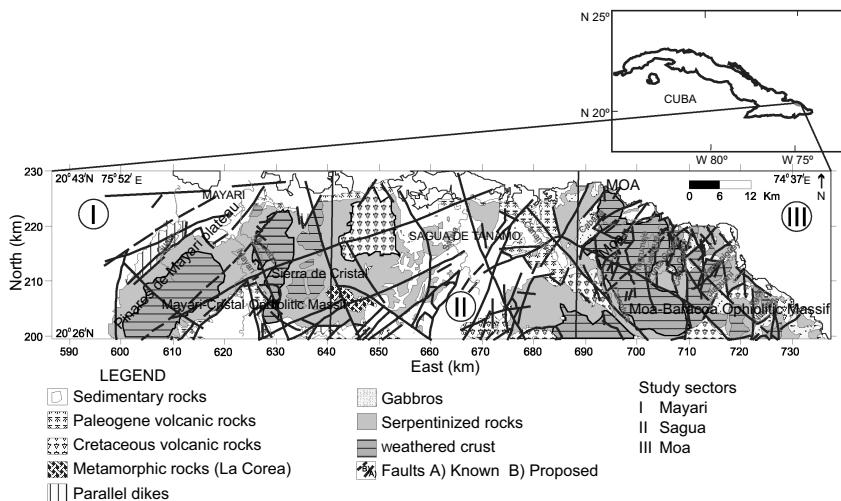


Figure 1. Location of the study area showing the Mayari, Sagua, and Moa sectors of this study and their surface geology (Albear et al., 1988).

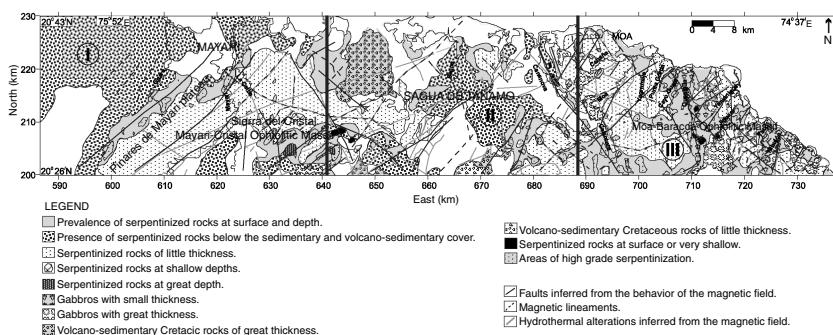


Figure 2. Qualitative geologic interpretation of the study area from aeromagnetic data (Batista, 2002).

In order to apply constraints on the unknown \mathbf{m} , we arrange equation 1 in a more convenient way.

$$d\mathbf{T} = \mathbf{T}(\mathbf{m}) - \mathbf{T}(\mathbf{m}_0) + \mathbf{A}(\mathbf{m}_0)\mathbf{m}_0 \equiv \mathbf{A}(\mathbf{m}_0)\mathbf{m}. \quad (2)$$

Using equation 2 we can express the following objective function,

$$F(\mathbf{m}) = \left\| d\mathbf{T} - \mathbf{A}(\mathbf{m}_0)\mathbf{m} \right\|_{C_d^{-1}}^2 + \left\| \mathbf{D}\mathbf{m} \right\|_{C_D^{-1}}^2, \quad (3)$$

where $F(\mathbf{m})$ is the objective function, and $\mathbf{D}\mathbf{m}$ is a matrix that contains the second derivatives of the depths with respect to x , y , and z . Minimizing the objective function, we find a model whose response fits the data (first term) and has minimum roughness (second term). Both terms were weighted by a diagonal covariance matrix for the magnetic data (C_d^{-1}) and for the model (C_D^{-1}). This latter term was kept constant for every interface. This allowed us to specify the roughness for each group of rocks. We maintained a constant diagonal matrix with diagonal elements given by a scalar we named the roughness factor (RF). We experimented with different values for RF, trying to fit the data as well as possible while producing a smooth model (minimum structure).

By quadratic programming, we minimized equation 3 subject to the following constraints on the unknown depths (Gill et al., 1986).

$$m_{\min} \leq m_i \leq m_{\max}, \quad (4)$$

where m_{\min} and m_{\max} are the minimum and maximum depths expected for every prism.

These constraints were used principally to prevent gaps between the groups and to allow us to specify which groups of rocks outcrop at surface and where. In this manner, the surface geology was incorporated in the inversion process. Although more information from previous exploration programs could be introduced to guide the model, in this case only surface geology and some borehole information were available.

If the data are rich enough, the first term of equation 3 predominates and large depth differences between prisms may be modeled. However, if the data do not have sufficient resolving power, then the effect of the second term of equation 3 can increase to the extent that it negates these depth differences, thus producing smoother features where the data is less rich. This problem occurs in areas of poorly distributed data or in the deepest parts of the model. Rejecting excessive roughness gave us some certainty because when a dip change appeared in the model, it was a dip change that was required by the data and remained despite the smoothing.

DATA AND INITIAL MODEL

On the basis of their geologic features and economic importance, we divided the study area into three sectors; the Mayari, Sagua, and Moa sectors (Figure 1). The aeromagnetic survey consisted of 320 north-south flight lines, with 500-m spacing and an average recording height of 70 m above the topographic surface. Data were corrected for diurnal variation and regional geomagnetic field

(IGRF-80 model; Chang et al., 1990; Chang et al., 1991). Figure 3 shows the magnetic anomaly at an elevation of 70 m after the typical corrections and then upward continued to 850 m. Most of the magnetic highs correspond to outcrops of serpentinized peridotites.

The petrophysical characterization of the ultrabasic rocks in eastern Cuba (Rodríguez, 1982) and in the northeastern region (Batista, 2002) of the Moa-Baracoa ophiolitic massif (Zamashikov and Tobachkov, 1971; Chang et al., 1990; Chang et al., 1991) shows that the largest susceptibilities are derived from mantle peridotites in the ophiolitic column (Table 1; mainly ultrabasic serpentinites). These have a mean value of 1423×10^{-6} SI (Table 1). Gabbros are the next highest with a mean of 107×10^{-6} SI and the volcano-sedimentary basement has a similar mean of 100×10^{-6} SI. Sedimentary rocks have the lowest mean value of 50×10^{-6} SI. The highest contrasts are between serpentinized peridotites and other rocks. A better estimation of the interfaces between these rocks is expected to be achieved through the inverse process.

From the magnetic susceptibilities shown in Table 1 it was possible to distinguish four groups of rocks as follows:

- group 1: Sedimentary rocks, Paleogene volcano-sedimentary rocks, La Corea metamorphic rocks, and parallel complex dikes
- group 2: Gabbros
- group 3: Serpentinized peridotites
- group 4: Cretaceous volcano-sedimentary rocks.

Each sector was modeled using the above four groups of rocks. The Mayari sector consisted of 432 prisms per group (432×4 for the four groups). The Sagua sector had 400 prisms per group, and the Moa sector had 384 prisms per group. In each sector, the horizontal

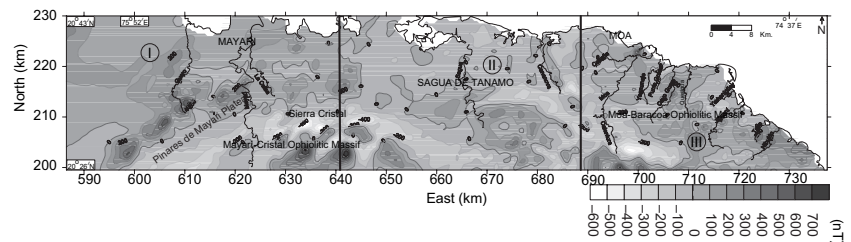


Figure 3. Aeromagnetic anomaly map of the study area. The original data (70 m) were upward continued to 850 m.

Table 1. Magnetic susceptibility of principal rocks in the northeastern Cuba region (Zamashikov and Tobachkov, 1971; Rodríguez, 1982; Chang et al., 1990; Batista, 2002).

Rocks type	Rock group	Number of samples	Range $\times 10^{-6}$ SI	Mean $\times 10^{-6}$ SI	S. deviation $\times 10^{-6}$ SI	Magnetization $\times 10^{-4}$ A/m
Sedimentary	Group 1	110	0–600	50	38	17.3
Gabbros	Group 2	382	10–900	107	328	37
Serpentinized peridotites	Group 3	736	10–9150	1423	282	515
Volcano-sedimentary	Group 4	300	0–890	100	102	34

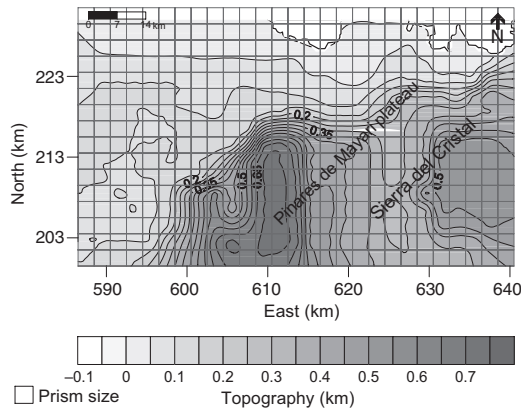


Figure 4. Surface topography of the Mayari sector. The grid represents the horizontal distribution of the prisms; each prism has a 2×2 km horizontal cross section.

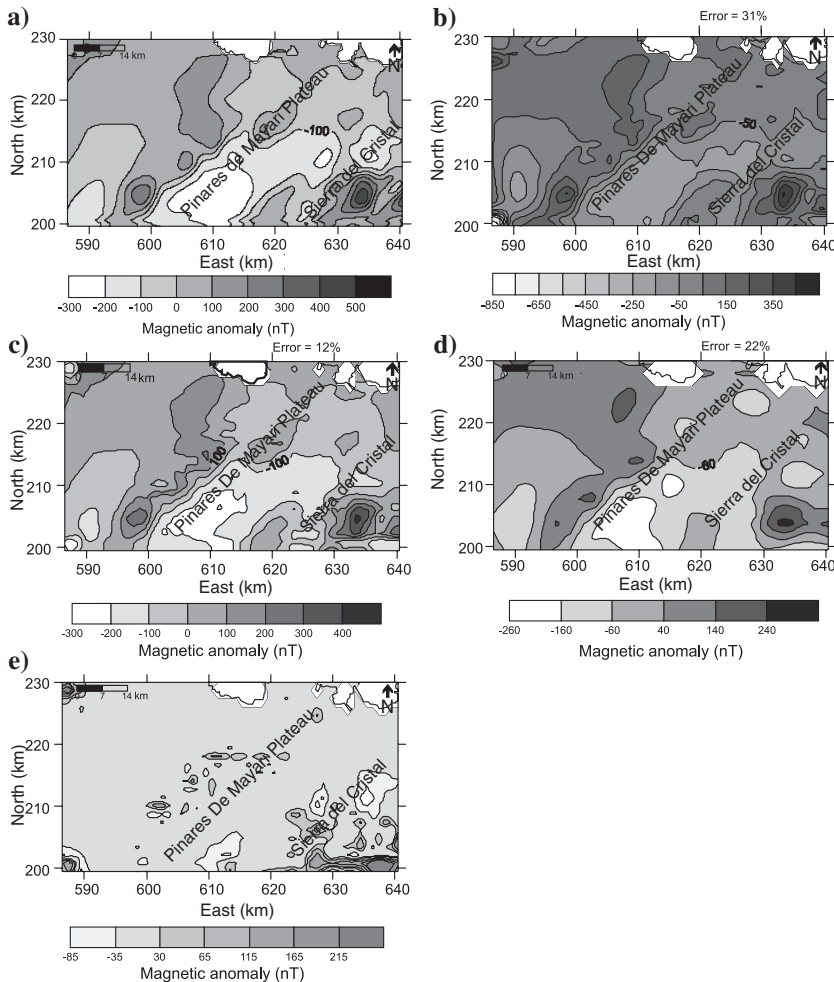


Figure 5. Measured magnetic anomaly and modeled responses for the Mayari sector: (a) upward-continued magnetic anomaly map, (b) magnetic response at the same elevation for the model with $RF = 10^{-1}$ (misfit = 31%), (c) response with $RF = 10^{-2}$ (misfit = 12%), (d) response with $RF = 10^{-3}$ (misfit = 22%), (e) difference between the measured magnetic anomaly and the response of the best model ($RF = 10^{-2}$).

cross section of every prism (2×2 km) was kept constant during inversion, but the top and bottom depths of the prisms changed. To minimize edge effects, we surrounded each modeled sector with a pseudo layer with an average susceptibility derived from the inversion process (e.g., sea floor, land). Surface geology (Albear et al., 1988, Figure 1) was used to determine where the rock groups outcrop in order to constrain the iterative solution. From available geologic data, we inferred the minimum and maximum depths for the top and bottom of each rock group. The differences between the minimum and maximum depths were large enough to permit a realistic variation of the topography of each group. Maximum depths for the rock groups were taken from previous geophysical and geologic studies (Fonseca et al., 1985; Batista, 2002; Marchesi et al., 2003). We used maximum thicknesses of 0.4 km for sediments (group 1), 0.6 km for gabbros (group 2), 6 km for serpentinized peridotites (group 3), and 10 km for volcano-sedimentary rocks (group 4). For outcropping prisms we used the elevation given by the average topography over the prism. The sea was considered nonmagnetic and

prisms located at the seabed were assigned to the underlying sedimentary group with an average depth of 50 m to the top of the prism. An initial program was needed to arrange the hundreds of prisms according to numerous factors including topography, surface geology, and maximum and minimum depths. The initial model used the mean values between the minimum and maximum depths and the mean thickness for every rock group. Only induced magnetization was considered, because remanent magnetization was not measured (Rodríguez, 1982).

The results using several experimental RF values in modeling the Mayari sector (Figure 4) are shown in Figure 5b-d. We selected $RF = 1 \times 10^{-2}$ because the data fit was good and a relatively smooth model was obtained. Figure 5e shows the difference between the best model response (Figure 5c) and the measured data. Very low values are seen over most of the map area, except in the corners. The inversion process for each sector took an average of 25 iterations to fit the data and required approximately four hours and close to 1024 MB of RAM on a Pentium III PC. With these results it was possible to plot maps of thickness and depth for every group of rocks and to confirm that surface geology was adequately taken into consideration in the final 3D model.

Similar inversions were carried out for the other two sectors. Model responses were compared with measured data and showed good agreement. An experimental inversion over the complete study area using 10×10 km prisms was also completed. It showed similar results, but with much less detail. Several north-south and east-west 2D cross sections over the 3D model were extracted to better understand structural behavior. Only the most important 2D cross sections are illustrated here, but the whole set was used to infer the positions of newly proposed faults.

RESULTS

Mayari sector

Group 3 rocks outcrop in the central and eastern parts of the Mayari sector and there are sediments at surface over the rest of the sector (Figure 1). The topography is relatively smooth in the northwest with steeper slopes in the central and eastern parts, which are known as the Pinares de Mayari Plateau and Sierra del Cristal, respectively (Figure 4). The upward-continued magnetic field exhibits high negative values in the central and eastern parts of the sector (Figure 5a), which are related to group 3 magnetic rocks of the plateau and sierra. According to Batista (2002), these negative values indicate a smaller thickness of group 3 peridotites, but our inversion suggests that in the northwest of the sector they represent thin serpentized peridotites underlying sediments (Figure 2).

Figure 5e shows the difference between the measured magnetic anomaly data and the best model. Random low values, except in the southeast, suggest the model provides a good fit.

Figure 6 shows the bottom topography obtained from the inverted 3D model for each rock group in the Mayari sector. All of the groups of rocks dip to the northwest in this sector. Group 3 rocks intrude groups 1 and 2 rocks (zero contour in Figure 6a and b). Serpentized peridotites (Figure 6c) are shallow in the same area as mentioned by Batista (2002), but are thick enough to produce the negative values shown by the magnetic anomaly map. The maximum thickness of the group 2 gabbros is 0.7 km and it reduces to zero where serpentized peridotites outcrop. The ophiolites (groups 2 and 3) have maximum thickness in the northwest and are also relatively thick to the south of Sierra del Cristal (Figure 6b and c). These variations of thickness were not predicted by Batista (2002).

Uplift of the Pinares de Mayari Plateau eroded the upper part of the geologic structures so that the ophiolitic rocks are thinner there (Figure 6b and c). Thicker ophiolitic rocks are responsible for the positive values of the magnetic anomaly map (Figure 5a). The uplift of the volcano-sedimentary basement (group 4) to the surface at the Pinares de Mayari Plateau produced the negative magnetic anomalies observed there (Figures 5a and 6c).

Correlation of structural information (Figure 1) with the depth maps shows a direct relationship between the steeper slopes shown in the inverted topographies and the main faults previously reported — mainly the northeast- and northwest-trending faults near the Pinares de Mayari Plateau. These fault systems are responsible for development of the horst reported by Campos (1983) that resulted in uplift and erosion of the upper groups.

Ten north-south and 4 east-west cross sections (Figure 6a) were analyzed to determine the dips of the interfaces between the modeled groups and to better understand the correlation of the model with the main faults that had been previously reported. Figure 7 shows a perspective view of the 3D model based on Sections 1 and 11 (Figure 6a), which traverse the model in the north-south and east-west directions, respectively. Combining these sections shows how the groups of rocks are tridimensionally arranged and that they are uplifted where surface geology indicates they should be. There is also a good match between previously mapped faults and the dip inflections along the interfaces of the different groups, suggesting that the 3D inversion provides a good representation of both the continuation of the faults at depth and the structural relationships of the groups. Previously unrecognized faults were also identified from the analysis of the complete set of cross sections (Figure 6a). None of these new features were identified by the previous qualitative model (Batista,

2002). More structural deformation is evident in the east-west direction than in north-south direction, even though the data was recorded along north-south flight lines. This demonstrates that 3D inversion is more appropriate than traditional 2D inversion.

Section 1 (Figure 7) shows group 1 sediments have a maximum thickness of about 1 km. They are underlain by a thin layer of gabbros that thins southward, and the group 3 serpentized peridotites

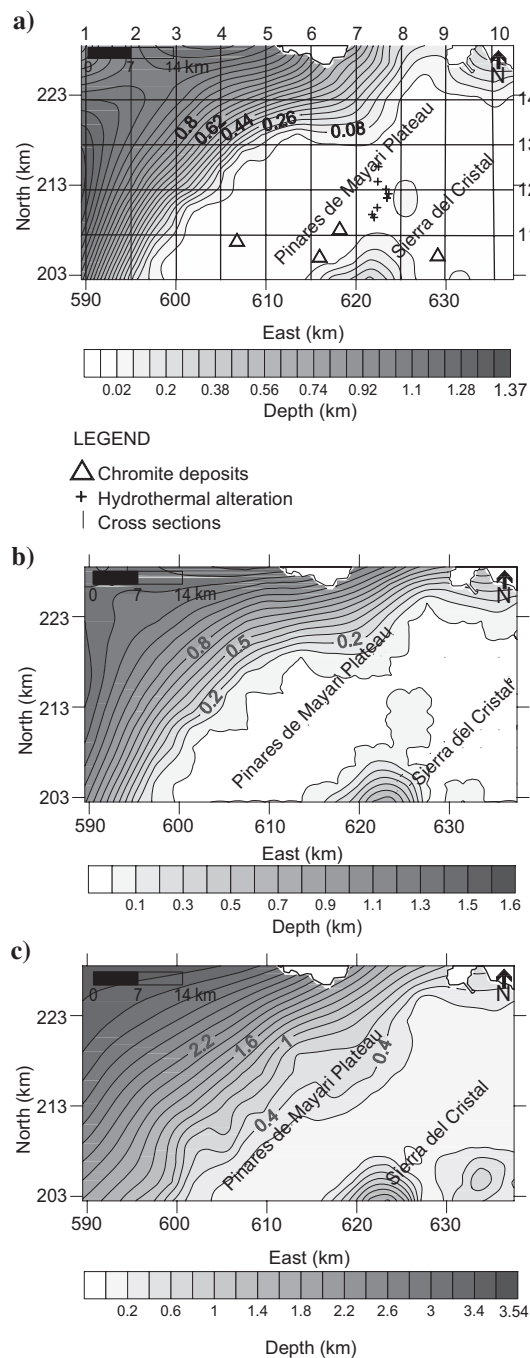


Figure 6. Bottom topography estimated by 3D inversion for the three uppermost rock groups in the Mayari sector: (a) group 1, mainly sedimentary rocks. Vertical and horizontal lines show the location of cross sections used for detailed analysis. (b) Group 2, gabbros; (c) group 3, ophiolites.

thicken to around 2.5 km thickness in the north. The northward deepening may indicate that uplift was predominant in the south.

Section 11 (Figure 7) shows that serpentized peridotites are exposed on the plateau. This section shows more faults than section 1, uplift of the volcano-sedimentary basement at the center of the cross section, and the erosion of group 1 sediments. Sediments thicken westward, suggesting that there is a basin developed to the west.

Taking into account the 14 cross sections and the depth maps for each group, the negative values of the magnetic anomaly map in the west, northwest, and north of the Mayari sector are consistent with

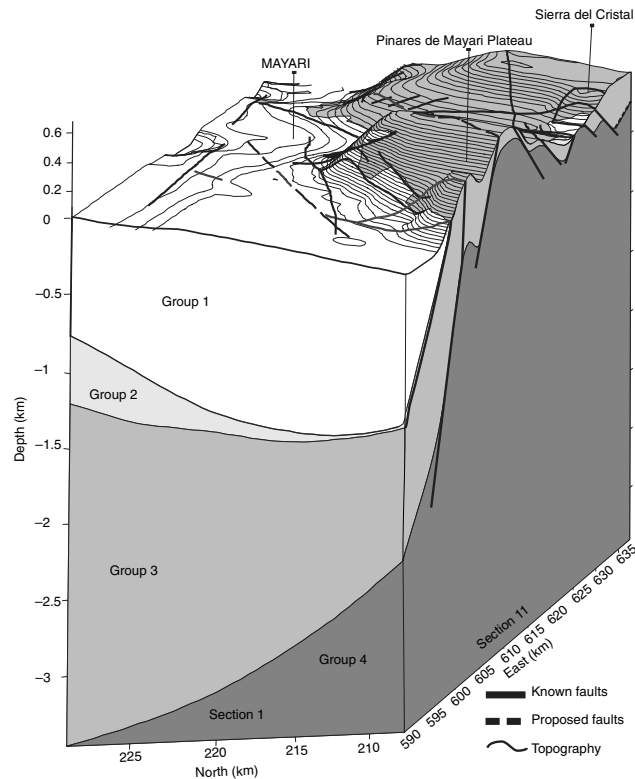


Figure 7. Perspective view from the Mayari sector 3D model showing the geometry of the four groups and their correlation with surface geology, previously mapped faults, and newly proposed faults.

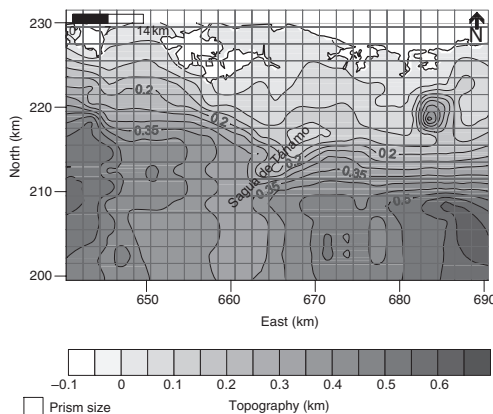


Figure 8. Surface topography of the Sagua sector. The grid represents the horizontal distribution of the prisms; each prism has a 2×2 km horizontal cross section.

the existence of a thick layer of serpentized peridotites below the nonmagnetized sediments. This suggests that the serpentized peridotites may extend northwest to the Holguín Massif, and supports the hypothesis of Cobiella et al. (1984) that they are a single body at depth, and are thus part of the massif.

Previous structural studies (Iturralde-Vinent, 1996; Echevarría-Rodríguez et al., 1991) have reported the emplacement of oceanic crust (ophiolitic rocks) from south to north by overthrusting on the continental crust. Our 3D model shows that structural deformation is greater in the east-west direction than in the north-south direction in the Mayari sector, and the same phenomenon is evident in both the Moa and Sagua sectors. Therefore, we propose three alternatives: that emplacement advanced northward over preexisting rocks that had been deformed in the east-west direction, or overthrusting was inhomogeneous in the east-west direction, or further deformation occurred after emplacement of the ophiolitic rocks. The postemplacement deformation might have been a response to extensional forces in the east-west direction (mostly normal faults). The inversion process does not have the resolution required to accurately estimate the dips of the fault planes. More geochronologic data is needed to determine which of these hypotheses is valid.

Our 3D model shows that the thickness of ophiolites is greater than that proposed by Fonseca et al. (1985) and less than that proposed by Marchesi et al. (2003). Thus, our 3D model provides new information, some of which agrees with previous hypotheses, and some that does not.

From a mineral exploration perspective, it is very important to know the depth and thickness of the gabbros and serpentized peridotites, because chromite deposits are found in the transition zone between these rocks (the Moho Transition Zone). Known chromite deposits in this region (Figure 6a) are associated with a thin layer of serpentized peridotites where the overlying gabbros have been removed by erosion; therefore, using this 3D model it is possible to determine the distribution of the serpentized peridotites and identify areas where the gabbros have been removed, or almost removed. Batista (2002) reported that where there is evidence of hydrothermal alteration between a thin layer of peridotite and volcano-sedimentary basement, precious metals deposited from hydrothermal fluids are present. The 3D model shows areas with this combination of geologic features, but field inspection would be needed to identify hydrothermal signatures. Figure 7 clearly shows the zones of minor and major thickness for each rock group. Areas where group 3 rocks are thin are important; if there is also evidence of hydrothermal alteration, these areas are prospective for precious metals.

Sagua sector

The Sagua sector is characterized by outcrops of less-magnetized rocks (groups 1 and 4). Topographic relief is high in the south, and smoother toward the coast. The Sagua de Tánamo basin is in the center of the sector (Figure 8), and is a feature that distinguishes this sector from the others. Figure 9a shows that the measured magnetic field is mostly negative in the Sagua sector, except for small areas in the center, southwest, and west. Batista (2002) argued that there must be serpentized peridotites below the areas of positive magnetic anomalies (Figure 2).

The same inversion procedure was used as for the Mayari Sector. We used surface geology as a constraint (equation 4), tested several RF values, and aimed to achieve the best possible model without over-fitting (equation 3). Figure 9 shows the measured magnetic anomaly data, the best model, and the difference between them. The misfit (22%) shows a good match between the measured data and model. The difference plot shows a largely random distribution with some areas of misfit in the northeast and west, which indicates that in these areas there is less certainty in the depth estimation.

The Sagua de Tanamo basin is a well-defined basin; its center is marked in Figure 10c. The inversion showed that within the basin the sediments (group 1) have a maximum depth of 0.25 km (Figure 10a). Gabbros (group 2) have a maximum depth of 0.33 km (Figure 10b) and a maximum thickness of 0.13 km. Serpentinized peridotites (group 3) have a maximum depth of 0.8 km (Figure 10a) and a maximum thickness of 0.5 km. There is also a small area in the southwest, away from the basin center, where the serpentinized peridotites deepen and thicken. In areas where group 2 gabbros are thin, the prospectivity for chromite deposits increases.

Fourteen cross sections were constructed, 9 in the north-south direction and 5 in the east-west direction (Figure 10a). Two cross sections and one 3D perspective view are particularly relevant (Figure 11). The 3D view shows a good representation of the basin. As was the case for the Mayari sector, the surface geology constrains the model very well and the previously mapped faults can be correlated with dip inflections of the interface between groups at depth. The geometry of the basin and its flanking normal faults can be seen, although it is not clear how the faults have controlled the basin over time. Nevertheless, the basin center has been displaced vertically by at least 800 m. Positive magnetic anomaly values over the basin (Figure 9a) are not because of the shallowness of the serpentinized peridotites (Batista, 2002), but to their thickness.

Some of the dip inflections of the interfaces between rock groups correspond with known faults, and a previously unknown fault is proposed in the north (Figure 11). Group 3 rocks are deepest (0.92 km) at the center of the basin (Figure 10c). In the west, serpentinized peridotites are thinner and in contact with the volcano-

sedimentary basement, which provides favorable conditions for hydrothermal activity and the development of precious metal mineralization (Figure 10c).

Moa sector

Magnetic rocks of group 3 are exposed over most of the Moa sector, which is characterized by an abrupt increase in topographic relief in the south (Figure 12). Figure 13 shows the measured magnetic field, the magnetic response from the best model, and the differences between them. The measured data and modeled magnetic response match well, with random small differences (Figure 13c). The magnetic anomaly map shows negative values in the west in the area where Batista (2002) suggested the serpentinite sequence was thin (Figure 2).

Figure 14 shows the modeled depths to the base of groups 1–3. For group 1 (Figure 14a), only minor variations of depth are apparent in areas where sediments are exposed (Figure 1). Gabbros (group 2) near the center of the sector are aligned in the north-south direction (Figure 14b) with a maximum depth of 0.25 km and maximum thickness of 0.12 km. Serpentinized peridotites (group 3) outcrop over most of the Moa sector, and at depth show a northwest-southeast alignment with a maximum depth of 0.9 km and a maximum thickness of 0.3 km (Figure 14c). In the west, the thickness of group 3 rocks is approximately 100 m, which is as predicted by Batista (2002). Two representative cross sections are shown on a 3D perspective view (Figure 15). Most of the exposed rocks are serpentinized peridotites, and there is good agreement between the modeled structures and previously known faults, and with the shallow depth of the group 4 volcano-sedimentary rocks. This sector shows a thin (0.2 km) near-surface layer of gabbros, which is important for chromite exploration, because the absence of gabbros at the Moho Transition Zone is an indicator of chromite mineralization, and here it is close to the surface. The 3D model of this sector shows a thinner ophiolite sequence than that reported in some previous studies (Batista, 2002; Marchesi et al., 2003). The Moa sector appears to be at the eastern extremity of ophiolite emplacement in the region.

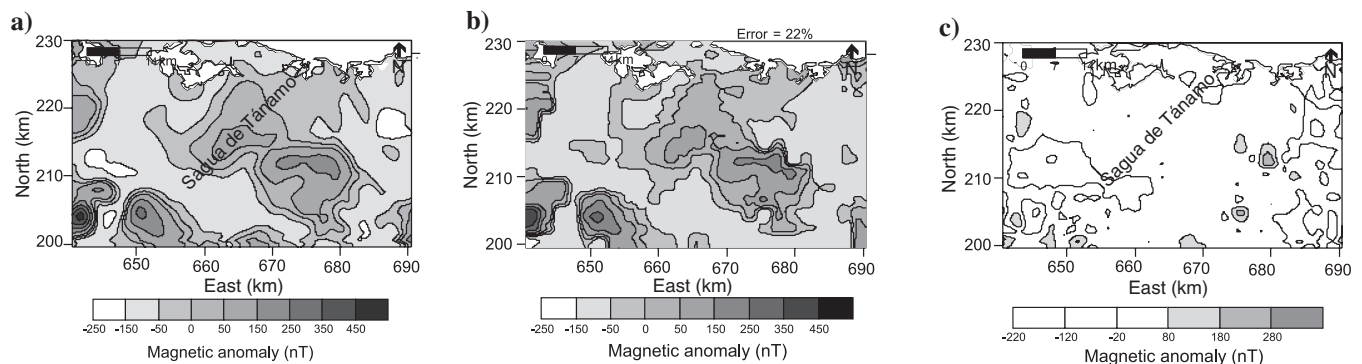


Figure 9. Measured magnetic anomaly map and modeled responses for the Sagua sector: (a) upward-continued magnetic anomaly map, (b) response from the best model with $RF = 10^{-2}$ (misfit = 22%), (c) difference between the measured magnetic anomaly and the response of the best model.

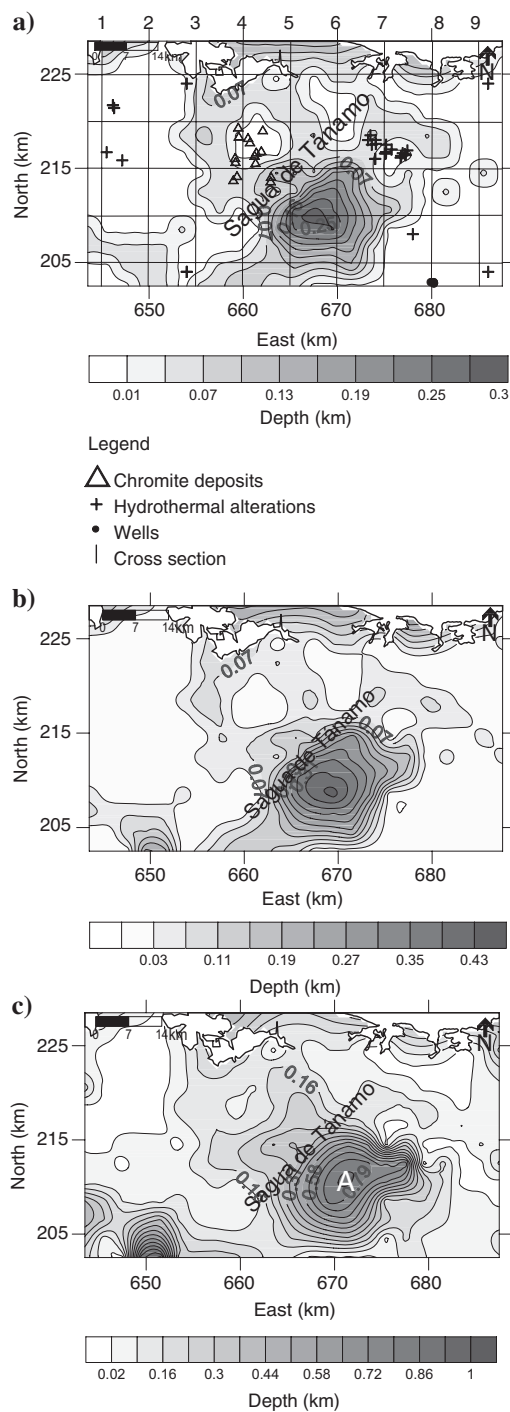


Figure 10. Bottom topography estimated by 3D inversion for the uppermost 3 groups in the Sagua sector: (a) group 1, mainly sedimentary rocks. Vertical and horizontal lines show the location of cross sections used for detailed analysis. (b) Group 2, gabbros; (c) group 3, ophiolites; A indicates the center of the Sagua de Tanamo basin.

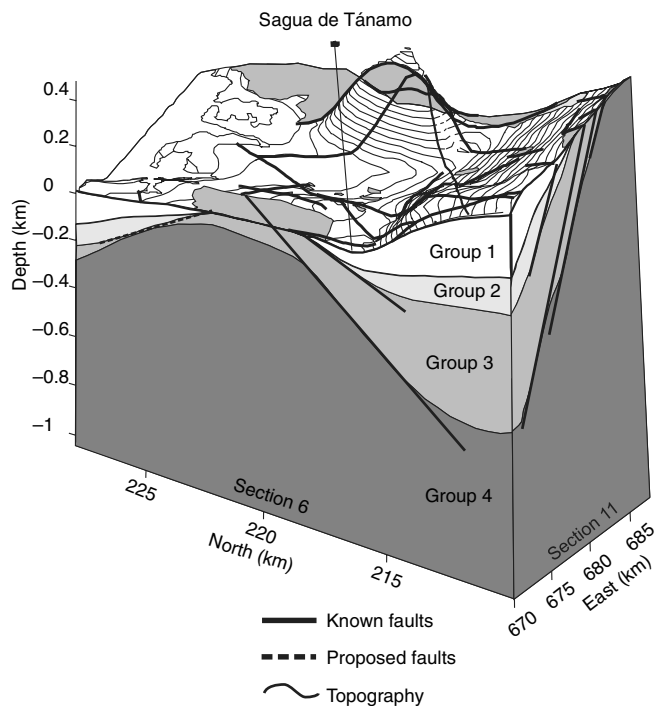


Figure 11. Perspective view from the Sagua sector 3D model showing the geometry of the four rock groups and their correlation with surface geology, previously mapped faults, and newly proposed faults.

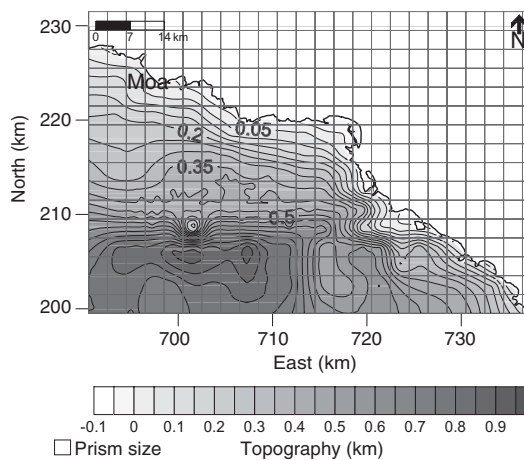


Figure 12. Surface topography of the Moa sector. The grid represents the horizontal distribution of the prisms; each prism has a 2×2 km horizontal cross section.

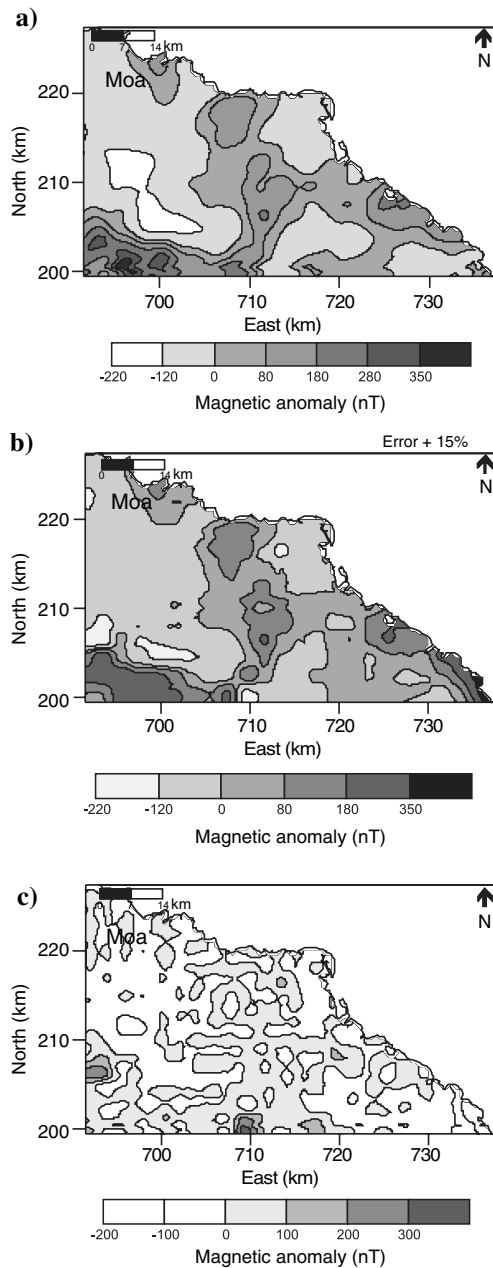


Figure 13. Measured magnetic anomaly map and modeled responses for the Moa sector: (a) upward-continued magnetic anomaly map, (b) response from the best model with $RF = 10^{-2}$ (misfit = 15%), (c) difference between the measured magnetic anomaly and the response of the best model.

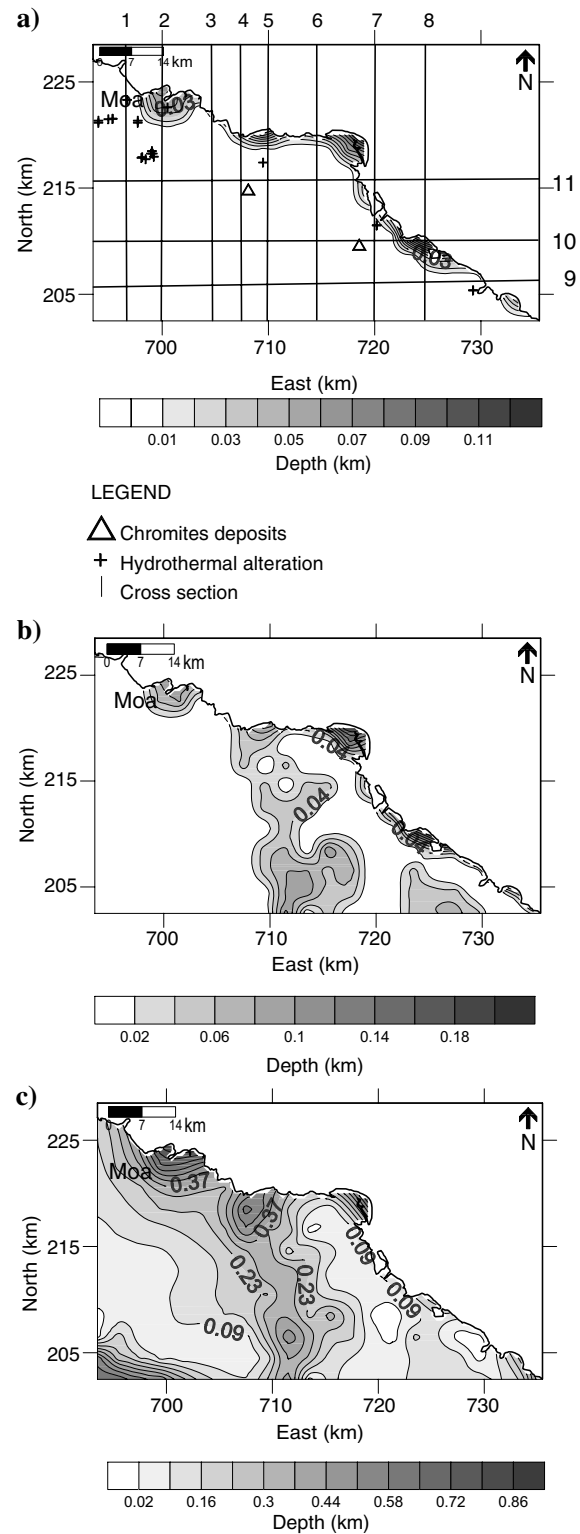


Figure 14. Bottom topography estimated by 3D inversion for the uppermost three groups of the Moa sector. (a) group 1, mainly sedimentary rocks. Vertical and horizontal lines show the location of cross sections used for detailed analysis. (b) group 2, gabbros; (c) group 3, ophiolites.

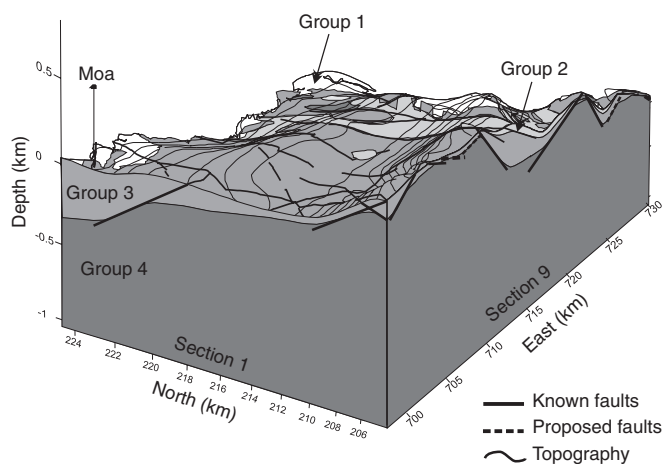


Figure 15. Perspective view from the Moa 3D model showing that the uppermost three groups are thinner than in the other sectors.

CONCLUSIONS

We used upward-continued magnetic anomaly data to obtain individual 3D models for each of the three sectors of the study area. We defined four groups of rocks according to their susceptibility contrasts. The iterative inversion process modeled the 3D bottom topography for each group of rocks and the solution was constrained according to the known surface geology and previous hypotheses about the maximum depths of the rock groups.

The method used for the 3D inversion took into account available geologic information, which reduced the nonuniqueness of the model solution and provided a more realistic model. The initial model was computed from the measured magnetic data, susceptibility contrasts, surface geology, and maximum depths and thicknesses of each group of rocks. The models were not over constrained and were not biased by predetermined hypotheses. The models demonstrated few similarities with a previous qualitative model. Most of the information obtained from our 3D modeling is new, and some of it contradicts previous findings. Our quantitative inversion provided better results than a previous qualitative analysis, mainly because the use of known geologic information constrained the solution and produced a more realistic model. There was good agreement between the surface geology and the modeled areas of structural uplift. Previously mapped faults correspond to dip inflections at the modeled interface between the defined rock groups. Other changes of dip at these interfaces are proposed as new faults that have not previously been observed or mapped.

The models for the three sectors of the study area are structurally different. The Mayarí sector is tectonically controlled by the Sierra del Cristal and the Pinares de Mayarí Plateau. In these areas, serpentinized peridotites thin and outcrop, suggesting that there has been uplift of the volcano-sedimentary basement and consequent erosion of the upper sequences. The depths of groups 1–3 rocks increase with distance from these structures and their thicknesses decrease coastward, which is consistent with the hypothesis that the ophiolites were overthrust from south to north.

The Sagua sector is characterized by the presence of a well-defined, 800-m-deep central basin. Overthrusting occurred during the Maestrichtian-Campanian (~70 Ma) at a rate of 1 mm every 88 years.

The Moa sector differs from the other two sectors in that the groups 1–3 are much thinner, and sedimentary rocks are almost entirely absent. Normal faults appear to be predominant, suggesting that extensional forces controlled the structural deformation of northeastern Cuba.

In all three sectors, areas where only a thin layer of serpentinized peridotites overlies the basement provide valuable targets for future prospecting as they identify the Moho Transition Zone, which is prospective for chromite exploration. Our 3D models show that the main structural deformation occurred in an east-west direction, suggesting that the north-south emplacement of the ophiolites was over preexisting east-west deformed continental rocks, or that overthrusting advanced inhomogeneously toward the north. It is also possible that there was east-west extensional deformation after emplacement of the ophiolites. Our modeling also showed that the thickness of each rock group appears to decrease from east to west across the entire study area.

ACKNOWLEDGEMENTS

We thank Joaquín Proenza for valuable comments on the geologic features of the study area. Our thanks go also to CICESE for their financial support of this project and to Humberto Benítez for support in the production of graphics.

REFERENCES

- Albear, J., I. Boyanov, K. Brezsnianszky, R. Cabrera, V. Chejovich, B. Echevarría, R. Flores, F. Formell, G. Franco, I. Haydutinov, M. Iturralde-Vinent, I. Kantchev, I. Kartashov, V. Kostadinov, G. Millán, R. Myczynski, E. Nagy, J. Oro, L. Peñalver, K. Piotrowska, A. Pszczolkowski, J. Radocz, J. Rudnicki, and M. L. Somin, 1988, Geological map of Cuba, 1:250 000: Academia de Ciencias de Cuba e Instituto de Geología y Paleontología.
- Batista, J., 2002, New geological regularities for the Mayarí-Sagua-Moa region departing from the aero-geophysics survey re-interpretation: Ph.D. thesis, Instituto Superior Minero Metalúrgico de Moa.
- Batista, J., A. Rodríguez, J. Blanco, and J. Proenza, 2002, Ophiolitic massif structure (NE Cuba), from the aero-magnetic survey: *Geologica Acta*, **37**, 369–387.
- Bhattacharyya, B. K., 1966, A method for computing the total magnetization vector and the dimensions of a rectangular block-shaped body from magnetic anomalies: *Geophysics*, **31**, 74–96.
- Campos, M., 1983, Principal features in tectonics from Holguín and Guantánamo eastern portion: *Minería y Geología*, **2**, 51–76.
- Chang, J. L., L. Corbea, F. Prieto, J. Hernández, and G. Brito, 1991, Results report for the aero-magnetic complex survey in Guantánamo and Holguín provinces (South Guantánamo sector): Technical report, Oficina Nacional de Recursos Minerales.
- Chang, J. L., G. Gribniyov, and A. Brodobo, 1990, Report about the result from the complex aero-magnetic survey in Santiago de Cuba, Holguín, Granma and Guantánamo provinces (Pinares de Mayarí sector): Technical report, Oficina Nacional de Recursos Minerales.
- Cobiella, J. L., 2000, Jurassic and Cretaceous geological history of Cuba: *International Geology Review*, **42**, 594–616.
- Cobiella, J. L., J. Rodríguez-Pérez, and M. Campos-Dueñas, 1984, East Cuba position in the Caribbean geology: *Minería y Geología*, **2**, 65–92.
- Echevarría-Rodríguez, G., G. Hernández-Pérez, J. López-Quintero, J. López-Ramos, R. Rodríguez-Hernández, J. Sánchez-Arango, R. Socorro-Trujillo, R. Tenreiro-Pérez, and J. Yparraquirre-Peña, 1991, Oil and gas exploration in Cuba: *Journal of Petroleum Geology*, **14**, 259–274.
- Fonseca, E., V. N. Zelepugin, and M. Heredia, 1985, Structure of the ophiolite association of Cuba: *Geotectonics*, **19**, 321–329.
- Gallardo, Luis A., M. A. Pérez-Flores, and E. Gómez-Treviño, 2003, A versatile algorithm for joint 3D inversion of gravity and magnetic data: *Geophysics*, **68**, 949–959.
- , 2005, Refinement of three-dimensional multilayer models of basins and crustal environments by inversion of gravity and magnetic data: *Tectonophysics*, **397**, 37–54.
- Gill, P. E., S. J. Hammarling, W. Murray, M. A. Saunders, and M. H. Wright, 1986, User's manual guide for Issol (version 1.0): A fortran package for constrained least squares and convex, quadratic programming: Department

- ment of Operations research, Stanford University, Technical report SOL 86-1.
- Iturralde-Vinent, M. A., 1994, Cuba Geology: A new plate-tectonic synthesis: *Journal of Petroleum Geology*, **17**, 39–70.
- , 1996, Cuban ophiolites geology, in M. A. Iturralde-Vinent ed., *Ophiolites and back-arcs from Cuba: IGCP project 364, Special contribution no. 1*, 83–120.
- Marchesi, C., J. Proenza, F. Gervilla, C. J. Garrido, J. C. Melgarejo, R. Díaz-Martínez, and M. Godard, 2003, New petrologic and structural constraints on the origin of the Mayarí-Baracoa ophiolitic belt (eastern Cuba): *Geophysical Research Abstracts*, **5**, 00278.
- Proenza, J., F. Gervilla, J. C. Melgarejo, and J. L. Bodinier, 1999, Al- and Cr-rich chromitites from the Mayarí-Baracoa ophiolitic belt (Eastern Cuba): Consequence of interaction between volatile-rich melts and peridotites in supra-subduction mantle: *Economic Geology*, **94**, 547–566.
- Rodríguez, A., 1998, Tectonics and geodynamics of the Moa region: *Minería y Geología*, **15**, 37–41.
- Rodríguez, J., 1982, Deep structural geology of eastern Cuba from geophysical data: Ph.D. thesis, Mining Institute of Leningrad.
- Zamashikov, M. E., and V. Tobachkov, 1971, Report about the search over the 1:50 000 map confined to the SE of hyper-basic Moa-Baracoa massif: Technical report, Oficina Nacional de Recursos Minerales.